Emission Optics of the Steigerwald Type Electron Gun

Chong-Yu Ruan, Manfred Fink

Department of Physics, The University of Texas, Austin, Texas 78712

Abstract

The emission optics of a Steigerwald type electron gun is re-examined. The virtual and real points of divergence, divergence angles and beam-widths of the electron beams at different telefocusing strength are measured in detail for first time . Two different Wehnelt cylinders are used to establish a contrasting viewpoint. The original 'focusing' curves measured by Braucks are reconstructed and will be explained only through a 'new' interpretation which is different from the conventional views. While the image of the emitting surface in front of the filament is indeed telefocused beyond the anode, the envelope of the beam does not 'focus' as expected. A new model for the emission mechanism is established based on our results.

1 Introduction

An electron gun with a telefocus Wehnelt grid was first proposed by K.H. Steigerwald in 1949[1] (see Figure 1). The focusing properties of this design are based on the shape of the equipotential lines inside the Wehnelt cylinder closely imitating a diverging and a converging lens combination. The name 'telefocusing' follows the optical analog. A detailed experimental verification of the predicted property was carried out by Braucks[2]. By changing the position of the inner Wehnelt cone (a) or the size of the outer Wehnelt opening (d_w), the strength of the two electron optical lenses will vary with the fields. As shown in Figure 2, Braucks demonstrated the telefocusing property of the Steigerwald type gun. The focusing distances (L_q) identified with the smallest beam diameter from the filament tip were plotted as a function of parameters d_w and a for his design. Changing the ratio d_w/a, the focal length could be varied at will. An intense electron beam that is naturally collimated without limiting apertures makes this gun very attractive for electron diffraction experiment.

Several authors have applied the Steigerwald type gun in gas phase electron diffraction units using counting techniques [3], [4], [5] and photographic plates(films)[6]. To get high count rates and keep the angular precision at the same time, it is advantageous that the beam is intense and narrow at the intersection of the beam and the gas jet, and the focal point of the beam is set at the entrance of the Faraday cage in the detecting plane[7]. In the telefocusing systems, the distance between two electrodes can be varied by the axial movement of the inner Wehnelt cone or the anode, thus allowing the focal distance to be adjusted and beam quality to be fine tuned. To investigate the effect influenced by the geometry of the lensing system, the beam profile at the proximity of the 'focal point' was measured and is discussed here for different combinations of a, D,

and d. It has already been pointed out by Schmoranzer et al.[8], and later investigated extensively by Schiewe et al.[9] that the sum $a + D$, i.e. the distance from the anode to the filament tip, strongly affects the focusing mechanism. We built a telefocus gun to probe the optics of an electrostatic analyzer. The measured magnification factors of the analyzer deviated significantly from the value one would expect based on computational simulation which was verified in several other ways. Two possibilities could account for this: the long established telefocusing theory could be wrong, or there could be an anomalous broadening in the analyzer that is responsible for the differences. Therefore diagnostic measurements have been setup to re-examine the electron beam generated from our telefocus gun, especially to find the focal points and the beam profiles in their proximity.

2 Experiments

2.1 Setup

As depicted in Figure 3, the telefocus electron gun was mounted on a movable stage which was able to move along the viewing line of a Faraday cage, whose entrance aperture was 50 micron. Two sets of deflector plates were placed between the gun and Faraday cage. The first set of deflector plates (aligner) moved along with the e-gun so that the emitting direction could be fine tuned. The second set of deflector plates (scanner) were attached to the detector, and a computer controlled power supply (Bertan 205B) was used to scan the beam over the aperture to investigate the size of the beam. The intensity profile of the beam was recorded with a Keithley 616 digital electrometer connected to a P100 computer through GPIB ports. The scans were taken at a 15mHz repetition rate. The emission

current from the electron gun was set to be in the range $\sim 1\mu A$. The beam profiles, which were always gaussian in shape, were measured at 5-7 different distances, ranging from L_e =90mm to 180 mm, in order to determine the divergence angle. The size of the beam could be determined in two different ways. The full width at half maximum (FWHM) was obtained by fitting the profile with a standard gaussian. The FWHM was compared with directly recorded half-maximum points. The two results agreed with each other within 5%. To determine the opening angle of the electron beam, the FWHMs from different positions were combined to track the envelope. However, in some extreme cases the beam profile became very broad that sweeping the beam could charge up the insulator behind the deflector plates. Furthermore the deflecting field became inhomogeneous, introducing additional error. To avoid this situation, we estimate the gaussian beam size by taking the inverse of the square root of the peak intensity and then calibrating the results with the cases where reliable scans were available. Since the peak intensity could be measured very accurately, the above method was an excellent method for extrapolating gaussian beam for larger beam diameters. Two different outer Wehnelt cylinders were used to investigate the effects due to field penetration. (A) Wehnelt had an opening of $d_w = 3.175cm$, and $d_w = 1.12cm$ was the value for (B) Wehnelt.

2.2 Results and Discussions

In all cases no focal points have been found. For all the adjustible range of the gun the FWHM of the beam investigated grew linearly with the distance between the gun and the detector (L_e). 3-dimensional plots of the beam-widths measured at different d_w/a over the range from $L_e = 0$ to $250mm$ were constructed for two Wehnelt cylinders. (Figure 4, 5) 'Point of divergence' can be defined as the point source on the symmetric axis where the beam intersects with the zero beam-width plane. The locations of these 'virtual sources'

points determine whether a real crossover appears along the beam path. Figure 6 shows that only in section marked (c) the real crossover appears in front of the filament; whereas in section (b), representing smaller beam-widths, the points of divergence are behind the filament. In section (c) the divergent lens contributes most strongly. Those crossovers should not be called 'focuses' as was recognized first by Braucks and later on confirmed by Schmoranzer et al.[8]. The beam-widths in (c) are actually larger than those in (b) along the observed distances. It is not clear whether a crossover will appear at larger distance as Braucks measured(Figure 2). We suspect that Schmoranzer et al. [8],[9] observed cuts at a fixed L_e value and the minimum beam-width was mistaken as 'focal point' of the beam. Figure 7 shows such cuts measured at $L_e = 93.2mm$. The origin of the coordinate system for L_e and the position of the inner Wehnelt cone is set at the front edge of the electron gun (Figure 3). By changing the d_w/a ratio in the gun, the size of the emitting surface and the divergence angle both change. The narrowest beam-width observed is the minimization due to the combination of both factors. In the proximity of the gun, the size factor dominates, but in the far field, the dispersion angle is more important. As supported by both Figures 4 , 5 we found that while moving the detector to larger L_e value, the minimum beam-width starts from a low d_w/a value then gradually moves toward a particular d_w/a value with the lowest dispersion angle. This actually agrees with one of the features in Braucks' original plot (Figure 2) where the d_w/a values, corresponding to increasing 'focal lengths' (L_q), converge at one point. To support our argument, we inserted into Braucks' plot our measurements, using L_q as the distance from the filament to the detector, the minimum beam-width was achieved by tuning d_w/a. Figure 2 shows that the d_w/a values actually agree with Braucks' measurements. Another feature we reproduced well is that the 'density' of the function $f(L_q, d_w/a)$ grows at lower d_w. However, the density of f in our measurement is much greater than Braucks'.

One possible way of explanation may come from D, the distance from the anode to the Wehnelt cylinder. As pointed out by Schmoranzer and Schiewe, the value of $(D + a)$ is a good parameter in the 'focusing' mechanism[9]. The d_w/D values in our setup were larger than those Braucks used. That means our converging field is stronger inside the Wehnelt cylinder while the diverging field is weaker. Since the spreading of L_q curves in Braucks' plot was the result of telefocusing mechanism, it may be reasonable to link the increased density to our stronger convergent fields.

The telefocusing lenses do exist in the Wehnelt cylinder, but a complete ray tracing which simulates the beam emission process has never been realized as in other gun types [10]. The general dispersion angle involved in this case is in *mrad* range, which is difficult to simulate; the uncertainty in the initial conditions poses a fundamental problem. A reverse field created by the self-biasing and the kinetic energy of the thermal electrons defines a zero energy surface. This surface, not the filament, serves as the emitting object in the imaging system of a telefocusing gun. The shape of this surface depends mostly on the local symmetric mechanical design and the electron-electron interaction, but not on the shape of the filament. This explains why the electron beams are circular while the hair-pin filament is elongated in one direction. The emission current would increase exponentially as a decreases however the zero energy surface grows due to a greater reverse field created by the self-biasing resistor, and vice versa.

In Figure 6, the point of divergence appears in front of the filament only for small values of d_w/a when a is rather large (marked as section c). For very high d_w/a (section a), the emitting surface is fully exposed to the anode and no crossover will appear. In the intermediate d_w/a range (section b) a minimum beam-width might be obtained, but no crossover has to occur. This avoids the 'Boersch' effect coming from the Coulombic electron-electron repulsion at the crossover[11], and ensures the fact that the beam

divergence angle can be kept very small at high emission current.

As shown in Figure 8, it is interesting to note that in many cases the relative momentum spread ($\delta p/p$) in phase space, which defines the dispersion angle α for each ray bundle emitted from emitting surface, is smaller than the thermal broadening, $\alpha_T = \sqrt{kT/eV} \sim 4.18 \times 10^{-3}$ rad. Particularly for Wehnelt cylinder (A), the average transverse velocity of the thermal electrons is reduced by a factor of 10 at the minimum beam-width condition. Generally in a simplified treatment one assumes that the transverse velocity distribution changes only little in the emission process, however this is only true for electrons leaving the charge cloud perpendicularly. In the transverse direction, the equipotential lines of the local reverse field act as filters and reduce the emittance angles. It also indicates that the angular spread of the beam envelope is mostly from the inherent thermal broadening than from the lensing process in the gun. Therefore by using filament with lower operating temperature, e.g. barium oxide, hexaboride cathodes, beams with smaller angular spread can be obtained. It is noteworthy that in section (b) marked in Figure 6, the electron would acquire highest brightness since both beam-width and dispersion angle were minimized.

The answer to why the beam envelope created by a telefocuing electron gun does not converge actually can be illustrated also by its optical analog. In a telescope, the remote object is imaged upon the eye through a telefocusing mechanism. The envelope of all the incoming light rays, traced back, is diverging as it will ultimately reach the star we are observing. Similarly for an electron gun, it should be that the image of the emitting surface be reconstructed remotely while the beam envelope as a whole keeps diverging. As will be discussed in more details in the following article, the very same electron gun with (B) Wehnelt is used to probe the imaging optics of a spherical analyzer. Two beam-profiles are measured very accurately at the entrance and exit of the analyzer. Based

on the measurements of the beam envelope obtained in this work, and the ratio of the two beam profiles, the location of the images could be deconvoluted. The position of the image of the emitting surface at different d_w/a is shown in Figure 9 where indeed the source to image distance (L_q) increases as the strength of the telefocusing increases(d_w/a decreases).

We propose a new model to describe the performance of a telefocus electron gun which is illustrated in Figure 10. In case (a) the inner Wehnelt cylinder is most retracted from the anode, the total emission is very low, and the reverse biasing field is rather weak. The emitting surface thus is very close to the filament and small; also a real crossover is observed to form in the gun. These two features facilitate a small beam size at the proximity of the gun, as shown in Figure 4. This geometry also creates the strongest diverging fields which account for the largest imaging length measured, as shown in Figure 9. Moving the inner cylinder further out, the real crossover withdraws toward the emitting surface. In case (b) the electron gun is on the verge of having a real crossover inside the Wehnelt cylinder. While the total emission current is increasing, the emitting surface begins to move out of the filament and grows in size. As the inner Wehnelt cylinder continues to be moved forward, the strength of the converging and diverging fields adjust accordingly. In case (c) the electron gun has the least spreading beam and correspondingly the furthermost virtual point of divergence. Total emission current grows further, and the larger emitting surface contributes to a wider beam-width in the proximity of the gun compared to case (a) but produces the narrowest beam in the far field due to its very small angular spread. No real crossover is present anywhere in the emission process. This relieves the energy broadening from coulombic repulsion force. As the inner Wehnelt cylinder is further moved forward, in case (d) , the emitting surface is greatly exposed to the anode voltage; the very weak diverging fields account for the shortest imaging length.

While the emission current is the greatest, the beam-width and the dispersion angle are also greatest in this geometry. Note that in case (c) the minimum beam-width condition is actually the interplay of the diverging and converging lenses inside the Wehnelt cylinder. Surprisingly, by reducing the self-biasing resistor and hence increasing the total emission current, the lensing fields do not change much. Also the growth of the emitting surface is insignificant as verified by a small increase in the beam-width. This weak response is caused by the very great potential gradient in the proximity of the emitting surface which downgrades the reverse biasing fields in this situation. The lensing fields obviously operate in larger scale and depend most critically on geometrical factors. Note that the spreading of the beam is highly exaggerated in Figure 10 to help illustrate the emission profiles. In reality, the overall beam envelopes and the singular emitting profiles coming from point sources on the emitting surface very much overlap with each other.

3 Conclusion

The very small dispersion angle found in (A) Wehnelt cylinder demonstrated the superb ability of telefocus gun to create a very narrow, well collimated and intense electron beam with very simple design. Our new model explains the changes in the emission optics of the Steigerwald type gun from generating focused beams to creating parallel beams. Throughout the investigation, the emission current of the electron gun was set to $\sim 0.1\mu A$ range to avoid complications due to Coulomb repulsion force at the emitting surface. It was found that the positions of points of convergence stayed within 10% while the current could be increased up to a factor of 100. Also our d_w/a values in Figure 2 agreed well to Braucks' results although the general structures of the electron guns were different. These two facts point to the possibility of studying the emission optics of the telefocusing

electron gun systematically based on geometric parameters (e.g. d_w/a, d_w/D) in spite of the fact that the emission surface can not be constructed reliably.

4 Acknowedgement

One of the authors wishes to express his gratitude to Dominik Hammer for helpful discussions, and to Chris Zernial for making the graphs of the emission optics. This work was supported by Texas Advanced Research Project and Robert A. Welch Foundation.

References

[1] K.H. Steigerwald, Optik **5**, 469(1949)

[2] F.W. Braucks, Optik **15**, 242(1958)

[3] M.Fink and R.A. Bonham, Rev. Sci. Instr. **41**, 389(1970)

[4] M.Fink, P.G. Moore and D.Gregory, J. Chem. Phys.**71**, 5227(1979)

[5] H.F. Wellenstein, H. Schmoranzer,R.A. Bonham, T.C. Wong, J.S. Lee, Rev. Sci. Instr. **46**, 92(1975)

[6] M. Taguchi and T. Iijima, Jpn. J. of Appl. Phys. **23**, 921(1984)

[7] B. Miller and M. Fink, J. Mol. Struct. **48**, 373(1978)

[8] H.Schmoranzer, H.F. Wellenstein, and R.A. Bonham, Rev. Sci. Instr., **46**,89(1975)

[9] B. Schiewe, H. Schmoranzer, and P. Wollenweber, Rev. Sci. instr., **48**, 893(1977)

[10] R. Hutter, Focusing of Charged Particles, **vol II**, Academic Press INC(1967); E. Munro, and H.P. Freund, Electron-Beam Sources and Charged-Particle Optics, SPIE Proc.(1995)

[11] B. Zimmermann, Adv. Electronics and Electron Physics **29**, 257(1970)

Figure 1: The Steigerwald type electron gun.(A)Filament, (B)Self-biasing resistors, (C)Outer Wehnelt cylinder, (D)The inner Wehnelt cone, (E)Anode.

Figure 2: The lines show the reconstruction of the L_q ('focal distance') curve based on Braucks' paper. The points have been extracted from our measurements.

Figure 3: Experimental apparatus: (A)electron gun; (B) and (C) deflector plates, (D) Faraday cage and aperture.

Figure 4: The 3D plot of the beam-widths over the distance and different d_w/a for Wehnelt cylinder (A).

Figure 5: The 3D plot of the beam-widths over the distance and different d_w/a for Wehnelt cylinder(B).

Figure 6: The point of divergence. Note that crossovers are formed when the points of divergences rise above the inner Wehnelt cone position (slanted line).

Figure 7: Beam-widths(FWHM) at $L_e = 93.2mm$

Figure 8: Beam dispersion angle.

Figure 9: The image positions as determined from the data with a spherical analyzer.

Figure 10: The electron beams emitted from a telefocus electron gun

This figure "fig1.jpg" is available in "jpg" format from:

http://arXiv.org/ps/physics/9905031v1

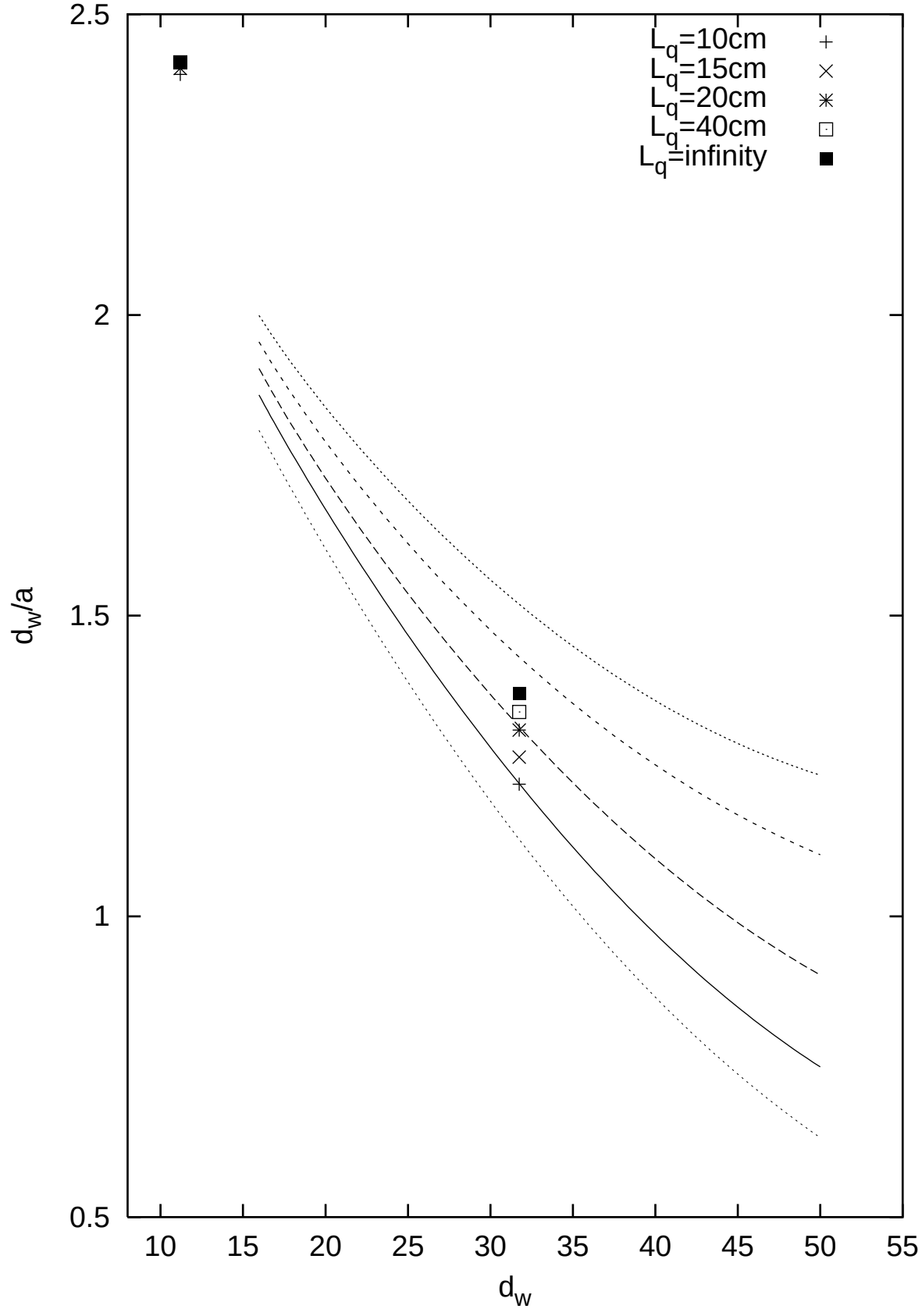
2.5
2
1.5
1
0.5
10
15
20
25
30
35
40
45
50
55
d_w
d_w/a
L_q=10cm
L_q=15cm
L_q=20cm
L_q=40cm
L_q=infinity

This figure "fig3.jpg" is available in "jpg" format from:

http://arXiv.org/ps/physics/9905031v1

This figure "fig4.jpg" is available in "jpg" format from:

http://arXiv.org/ps/physics/9905031v1

This figure "fig5.jpg" is available in "jpg" format from:

http://arXiv.org/ps/physics/9905031v1

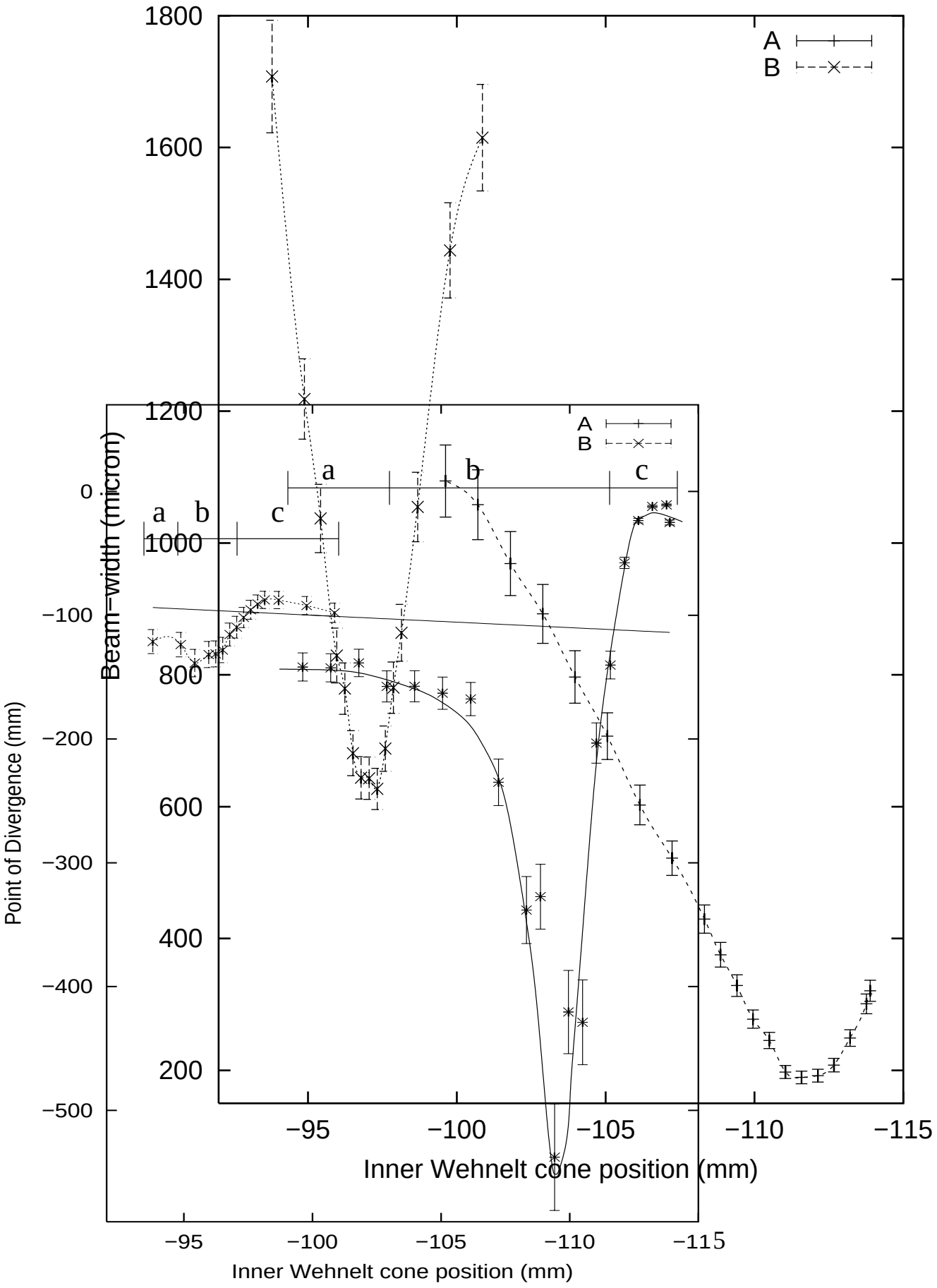
A
B
a
b
c
Beam−width (micron)
Point of Divergence (mm)
Inner Wehnelt cone position (mm)
1800
1600
1400
1200
1000
800
600
400
200
0
−100
−200
−300
−400
−500
−95
−100
−105
−110
−115

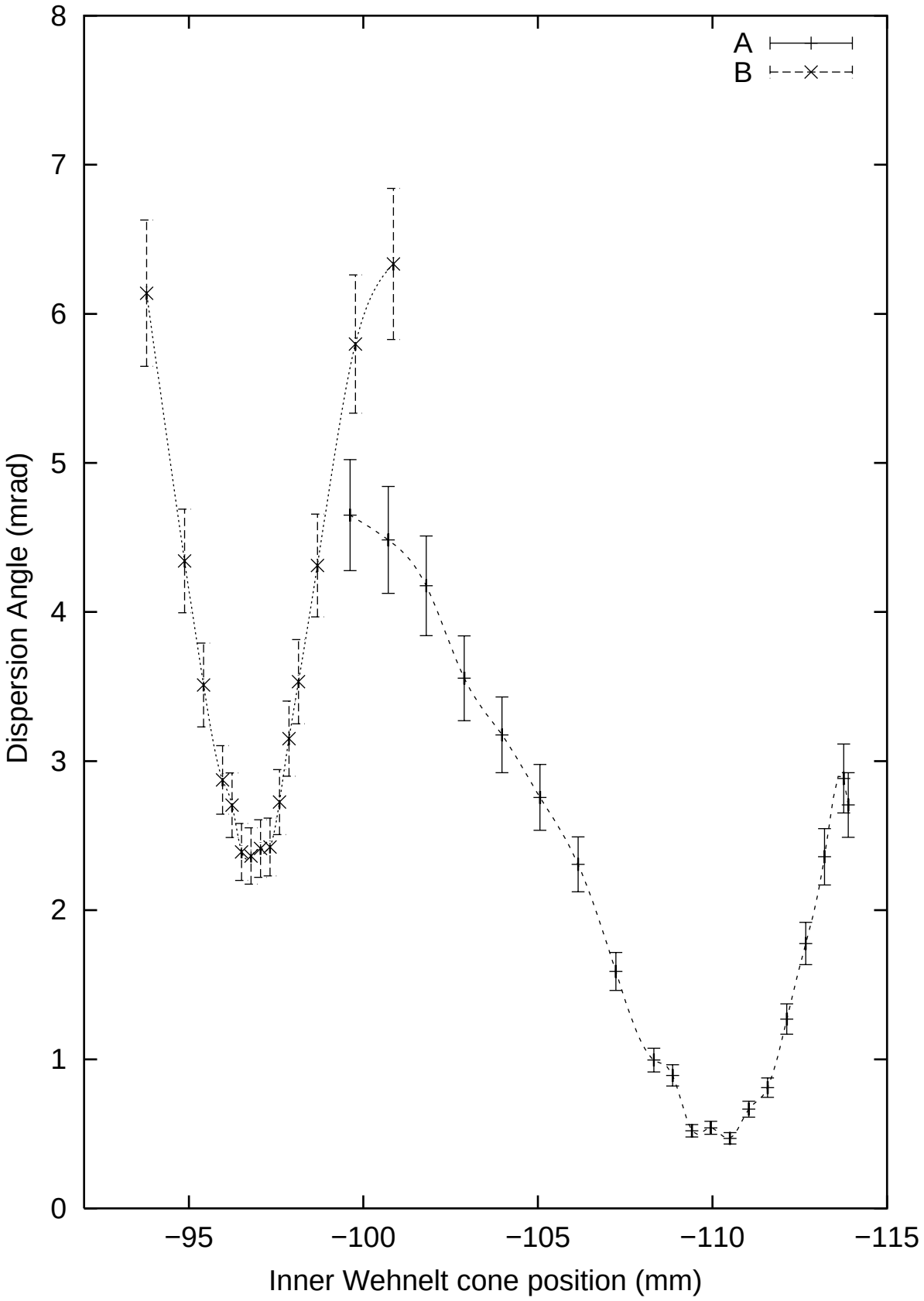
A
B
Dispersion Angle (mrad)
Inner Wehnelt cone position (mm)
0
1
2
3
4
5
6
7
8
−95
−100
−105
−110
−115

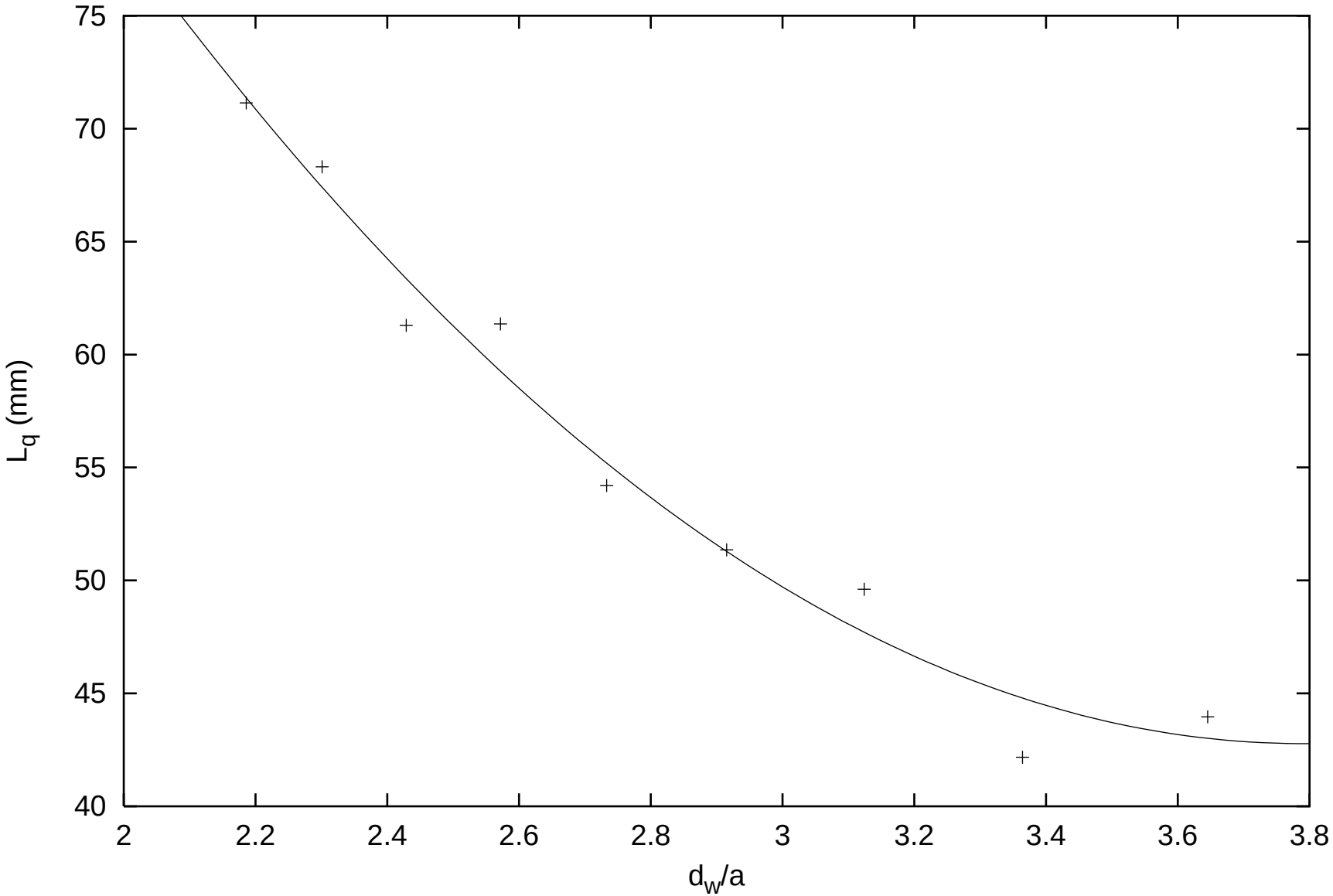
75
70
65
60
55
50
45
40
2
2.2
2.4
2.6
2.8
3
3.2
3.4
3.6
3.8
L_q (mm)
d_w/a

This figure "fig10.jpg" is available in "jpg" format from:

http://arXiv.org/ps/physics/9905031v1